Author Manuscript

Author Manuscript

Author Manuscript

Author Manuscript

HHS Public Access

Author manuscript

Sci Transl Med. Author manuscript; available in PMC 2017 January 25.

Published in final edited form as:

Sci Transl Med. 2016 August 31; 8(354): 354ra115. doi:10.1126/scitranslmed.aaf4891.

Pitx2 modulates a *Tbx5*-dependent gene regulatory network to maintain atrial rhythm

Rangarajan D. Nadadur[1], **Michael T. Broman**[2], **Bastiaan Boukens**[3,4], **Stefan R. Mazurek**[2], **Xinan Yang**[1], **Malou van den Boogaard**[4], **Jenna Bekeny**[1], **Margaret Gadek**[1], **Tarsha Ward**[5], **Min Zhang**[6,7,8,9,10], **Yun Qiao**[3], **James F. Martin**[6,7,8,9,10], **Christine E. Seidman**[5], **Jon Seidman**[5], **Vincent Christoffels**[4], **Igor R. Efimov**[3], **Elizabeth M. McNally**[11], **Christopher R. Weber**[1], and **Ivan P. Moskowitz**[1,*]

[1]Departments of Pediatrics, Pathology, and Human Genetics, University of Chicago, Chicago, IL 60637, USA [2]Department of Medicine, University of Chicago, Chicago, IL 60637, USA [3]Department of Biomedical Engineering, George Washington University, Washington, DC 20052, USA [4]Department of Anatomy, Embryology and Physiology, Academic Medical Center, Meibergdreef 9, Amsterdam 1105 AZ, Netherlands [5]Department of Genetics, Harvard Medical School, Division of Cardiovascular Medicine, Brigham and Women's Hospital, Boston, MA 02115, USA [6]Department of Molecular Physiology and Biophysics, Baylor College of Medicine, One Baylor Plaza, Houston, TX 77030, USA [7]Institute of Biosciences and Technology, Texas A&M Health Science Center, Houston, TX 77030, USA [8]Cardiomyocyte Renewal Laboratory, Texas Heart Institute, Houston, TX 77030, USA [9]Program in Developmental Biology, Baylor College of Medicine, Houston, TX 77030, USA [10]Cardiovascular Research Institute, Baylor College of Medicine, Houston, TX 77030, USA [11]Center for Genetic Medicine, Northwestern University Feinberg School of Medicine, Chicago, IL 60611, USA

[*]Corresponding author. imoskowitz@uchicago.edu.

SUPPLEMENTARY MATERIALS

www.sciencetranslationalmedicine.org/cgi/content/full/8/354/354ra115/DC1

Materials and Methods

References (33–39)

Author contributions: R.D.N. was involved in design execution, analysis of all experiments, wrote the manuscript, and performed statistical analysis. M.T.B. performed and analyzed whole animal electrophysiology and echocardiography and wrote the manuscript. B.B. performed and analyzed ex vivo optical mapping experiments and wrote the manuscript. S.R.M. performed and analyzed single cell electrophysiology experiments and wrote the manuscript. X.Y. analyzed genomics experiments and performed statistical analysis. M.v.B. performed and analyzed chromosome conformation capture and wrote the manuscript. J.B. performed and analyzed gene expression, chromatin immunoprecipitation, and cellular experiments. M.G. performed and analyzed whole animal electrophysiology and chromatin immunoprecipitation experiments. Y.Q. performed and analyzed ex vivo optical mapping experiments. T.W. performed and analyzed iPS cardiomyocyte experiments and wrote the manuscript. M.Z. performed and analyzed enhancer identification and in vitro cellular experiments. J.F.M. analyzed enhancer identification and in vitro cellular experiments and wrote the manuscript. C.E.S. and J.S. analyzed iPS cardiomyocyte experiments and wrote the manuscript. V.C. analyzed chromosome conformation capture experiments and wrote the manuscript. I.R.E. analyzed ex vivo optical mapping experiments and wrote the manuscript. E.M.M. analyzed whole animal physiology, in vitro assays, and wrote the manuscript. C.R.W. performed and analyzed cellular electrophysiology experiments and wrote the manuscript. I.P.M. was involved in designing, performing, and analyzing all experiments; wrote the manuscript; and performed statistical analysis. All authors approved the final version.

Competing interests: The authors declare that they have no competing interests.

Data and materials availability: The RNA and ATAC sequencing data from this study have been deposited in the Gene Expression Omnibus database.

Author Manuscript Author Manuscript Author Manuscript Author Manuscript

Abstract

Cardiac rhythm is extremely robust, generating 2 billion contraction cycles during the average human life span. Transcriptional control of cardiac rhythm is poorly understood. We found that removal of the transcription factor gene *Tbx5* from the adult mouse caused primary spontaneous and sustained atrial fibrillation (AF). Atrial cardiomyocytes from the *Tbx5*-mutant mice exhibited action potential abnormalities, including spontaneous depolarizations, which were rescued by chelating free calcium. We identified a multitiered transcriptional network that linked seven previously defined AF risk loci: TBX5 directly activated PITX2, and TBX5 and PITX2 antagonistically regulated membrane effector genes *Scn5a*, *Gja1*, *Ryr2*, *Dsp*, and *Atp2a2*. In addition, reduced *Tbx5* dose by adult-specific haploinsufficiency caused decreased target gene expression, myocardial automaticity, and AF inducibility, which were all rescued by *Pitx2* haploinsufficiency in mice. These results defined a transcriptional architecture for atrial rhythm control organized as an incoherent feed-forward loop, driven by TBX5 and modulated by PITX2. TBX5/PITX2 interplay provides tight control of atrial rhythm effector gene expression, and perturbation of the co-regulated network caused AF susceptibility. This work provides a model for the molecular mechanisms underpinning the genetic implication of multiple AF genome-wide association studies loci and will contribute to future efforts to stratify patients for AF risk by genotype.

INTRODUCTION

The transcriptional architecture that confers robustness to cardiac rhythm must tightly control cardiac channel gene expression, because increased or decreased channel expression can cause cardiac arrhythmias (1). Atrial fibrillation (AF), the most common human arrhythmia, is an irregularly irregular pattern of atrial depolarization resulting in uncoordinated atrial contraction. AF affects more than 33 million people worldwide and represents a growing cause of morbidity and mortality (2). Although most AF presents in the context of concomitant cardiac pathology, such as hypertension and heart failure, genome-wide association studies (GWAS) have identified a genetic predisposition underlying AF.

Human AF GWAS have implicated multiple transcription factors, including *TBX5* and *PITX2* in AF, raising the possibility that perturbations of a gene regulatory network for atrial rhythm control may underlie some AF susceptibility (3). Dominant mutations in the T-box transcription factor *TBX5* cause Holt-Oram syndrome, characterized by disrupted heart and limb development (4–6) and increased AF risk (6). GWAS has linked common sequence variants close to or intronic within TBX5 to prolongation of the PR interval—the time interval between the electrocardiogram (ECG) P wave and QRS, an AF risk factor—and, more recently, to increased AF risk itself (7–10). *PITX2*, a paired-like homeodomain transcription factor, plays a critical role in heart development and adult rhythm control. *PITX2* is the most frequently reported AF-susceptibility locus (3). Adult-specific *Pitx2* deletion in mice causes AF susceptibility and increased expression of ion channels linked to AF (11).

AF pathophysiology requires a cellular trigger event, which initiates inappropriate depolarization, and a fibrillogenic substrate, or abnormal myocardium that propagates the

Author Manuscript Author Manuscript Author Manuscript Author Manuscript

trigger. Most genetic loci implicated in AF encode ion channels that affect trigger frequency or substrate, but not both (3). Animal models based on disruption of these channels do not exhibit spontaneous AF in the absence of concomitant cardiac pathophysiology, and no mouse model of primary AF has been reported (12). We tested the hypothesis that adult-specific removal of *Tbx5* in the mouse may cause atrial gene regulatory network dysfunction and AF. This removal generated primary, spontaneous, and sustained AF in the absence of other cardiac pathologies. We identified a regulatory element at *PITX2* that was modulated by a canonical TBX5 binding site. *Tbx5* haploinsufficiency–induced transcriptional and myocyte abnormalities and AF susceptibility were rescued by *Pitx2* haploinsufficiency. We have therefore uncovered a multilevel gene regulatory network for atrial rhythm homeostasis, driven by TBX5 and repressed by PITX2, organized as a type 1 incoherent feed-forward loop (13). This transcriptional architecture links 7 AF GWAS loci in a single network, providing a molecular model for their genetic implication in AF risk.

RESULTS

Adult-specific *Tbx5* deletion causes rapid-onset AF

Tbx5 was deleted from the adult mouse by combining a *Tbx5* floxed allele (*Tbx5*^{fl}) (5) with a tamoxifen (TM)–inducible Cre recombinase allele at the Rosa26 (R26) locus (14). Mice homozygous for both alleles (*Tbx5*$^{fl/fl}$;*R26*^{CreERt2}) were treated with TM at 6 weeks of age, removing the T-box DNA binding region and ablating TBX5 expression (4, 5, 15). *Tbx5*-deleted mice developed an irregularly irregular heart rate 1 to 2 weeks after TM treatment. ECGs of ambulatory TM-treated *Tbx5*$^{fl/fl}$; *R26*^{CreERt2} mice showed a disorganized pattern of atrial activity compared to TM-treated *R26*^{CreERt2} controls (Fig. 1A). The absence of P waves in *Tbx5*$^{fl/fl}$;*R26*^{CreERt2} mice but not in controls was observed by signal-averaging ~1000 heartbeats (Fig. 1B). Poincaré analysis of the heartbeat, comparing successive beat lengths (using RR intervals, the time interval between sequential ECG “R” peaks), demonstrated stable intervals in controls but tremendous instability in *Tbx5*$^{fl/fl}$;*R26*^{CreERt2} mice, indicative of an irregularly irregular heartbeat and AF (Fig. 1C). Furthermore, a single atrial depolarization overlapped the surface P wave in *R26*^{CreERt2} controls, but multifocal irregular depolarizations were observed in *Tbx5*$^{fl/fl}$;*R26*^{CreERt2} mice by in vivo intracardiac electrograms 2 weeks after TM treatment (Fig. 1D).

We further interrogated the atrial arrhythmia by examining transmitral valve blood flow by pulsed-wave Doppler echocardiography. Transmitral valve blood flow demonstrated two phases: an “E wave” followed by an “A wave” in control *R26*^{CreERt2} mice, but the A wave was absent in *Tbx5*$^{fl/fl}$;*R26*^{CreERt2} mice (Fig. 1E). The absence of A-wave flow across the mitral valve is indicative of a lack of coordinated atrial contraction, a characteristic of AF. We observed AF by these metrics in 24 of 24 *Tbx5*$^{fl/fl}$;*R26*^{CreERt2} mice and in 0 of 10 *R26*^{CreERt2} mice ($P = 7.6 \times 10^{-9}$, Fisher’s exact test). These findings demonstrate spontaneous sustained AF in adult-specific *Tbx5*-mutant mice.

Cardiac function of *Tbx5*$^{fl/fl}$;*R26*^{CreERt2} mice at the onset of AF was unchanged compared to controls, with no difference in left ventricular ejection fraction observed in *Tbx5*$^{fl/fl}$;*R26*^{CreERt2} compared to *R26*^{CreERt2} mice 14 days after TM treatment (fig. S1). Ventricular conduction abnormalities, including monomorphic ventricular tachycardia (fig.

Author Manuscript Author Manuscript Author Manuscript Author Manuscript

S2A), polymorphic ventricular tachycardia (fig. S2B), and prolonged sinus pauses (fig. S2C), were observed; however, these arrhythmias were not present at the time of AF onset in *Tbx5*$^{fl/fl}$;*R26*^{CreERt2} mice and only manifested well after AF was observed in these animals, beginning ~3 weeks after TM treatment. Removal of *Tbx5* from the adult mouse therefore causes primary AF in the absence of left ventricular dysfunction or ventricular conduction abnormalities.

To assess atrial action potential (AP) propagation, we performed ex vivo optical mapping of intact adult mouse hearts (16). Adult-specific *Tbx5*-mutant mouse hearts demonstrated progressively slowed atrial conduction before AF (Fig. 1F). Atrial activation time was 13 ms at day 7, 20 ms at day 12, and >40 ms at day 14 after TM treatment in *Tbx5*$^{fl/fl}$;*R26*^{CreERt2} mice (Fig. 1F and movies S1 to S3). AP duration (APD) increased from 44 ± 4 ms to 53 ± 3 ms (120-ms pacing interval) at day 14 after TM treatment (figs. S3 and S4). Macro-reentrant arrhythmias were observed in *Tbx5*$^{fl/fl}$;*R26*^{CreERt2} mice with paroxysmal and sustained fibrillating patterns by day 14 (Fig. 1G). In contrast, *R26*^{CreERt2} control mice showed a uniform atrial activation pattern with no conduction slowing 14 days after the TM regimen (Fig. 1F). No paroxysmal or sustained AF was observed. Thus, removal of *Tbx5* slowed trans-atrial conduction fourfold between the first and second week after deletion, setting the stage for reentrant arrhythmias—an organ-level mechanism for AF.

Disrupted calcium flux causes abnormal cellular depolarizations in *Tbx5*-mutant atrial myocytes

Removal of *Tbx5* caused prolongation of APs and abnormal autonomous depolarizations in murine atrial cardiomyocytes. APs of atrial myocytes isolated from *Tbx5*$^{fl/fl}$;*R26*^{CreERt2} mice 7 days after TM treatment and paced at 0.5 Hz were significantly prolonged during phases 2 and 3 of the AP, compared to *R26*^{CreERt2} atrial myocytes (Fig. 2A); time to 90% repolarization (APD90) and 50% repolarization (APD50) were both prolonged. Early afterdepolarizations (EADs), delayed afterde-polarizations (DADs), and spontaneous triggered APs were all observed frequently in *Tbx5*$^{fl/fl}$;*R26*^{CreERt2} myocytes but never in *R26*^{CreERt2} myocytes isolated 7 days after TM treatment and paced at 0.5 Hz (Fig. 2B). These triggers are consistent with the initiation of paroxysmal AF, the most common form of AF (2, 17, 18). The aberrant depolarizations observed in isolated atrial myocytes provide evidence for an arrhythmic trigger after *Tbx5* removal.

Calcium-mediated inappropriate depolarizations of atrial myocardium have been implicated as an AF mechanism (1). Cytosolic calcium transients were prolonged in atrial myocytes isolated from *Tbx5*$^{fl/fl}$; *R26*^{CreERt2} mice but not *R26*^{CreERt2} controls 7 days after TM treatment (Fig. 2C). The decay constant, time to 50% decay, and time to peak were significantly prolonged in *Tbx5*$^{fl/fl}$;*R26*^{CreERt2} compared with *R26*^{CreERt2} atrial myocytes. To assess whether prolonged calcium transients were the cause of prolonged APs in *Tbx5*$^{fl/fl}$;*R26*^{CreERt2} atrial myocytes, we current-clamped isolated atrial myocytes after including the calcium chelator 1,2-bis(2-aminophenoxy)ethane-*N*,*N*,*N*′,*N*′-tetraacetic acid (BAPTA) (5 mM) in the intracellular solution. BAPTA rescued AP prolongation in *Tbx5*$^{fl/fl}$;*R26*^{CreERt2} atrial myocytes at APD50 and APD90 (Fig. 2D). Calcium chelation by BAPTA also rescued abnormal depolarizations in *Tbx5*$^{fl/fl}$;*R26*^{CreERt2} atrial myocytes (*P* =

Author Manuscript Author Manuscript Author Manuscript Author Manuscript

1.0 versus $R26^{CreERt2}$, $P = 1 \times 10^{-4}$ versus $Tbx5^{fl/fl};R26^{CreERt2}$, without BAPTA, by two-tailed Fisher's exact test) (Fig. 2D). Thus, disrupted calcium handling causes AP abnormalities in adult-specific *Tbx5*-mutant mice.

Adult specific *Tbx5*-deletion disrupts expression of AF-susceptibility genes

To explore the molecular mechanism underlying AF, we identified TBX5-dependent transcripts by RNA sequencing (RNA-seq) transcriptional profiling left atria isolated from $Tbx5^{fl/fl};R26^{CreERt2}$ and $R26^{CreERt2}$ 1 week after TM treatment, before the onset of AF. Numerous genes critical to atrial rhythm and about half of the genes previously linked to AF (3) were significantly down-regulated in $Tbx5^{fl/fl};R26^{CreERt2}$ left atria by RNA-seq (Fig. 3, A to C, and Table 1). Using RNA-seq, we noted significant down-regulation of numerous genes required for calcium handling, including *Ryr2*, *Atp2a2*, and *Sln* (Table 1). There was a modest and significant up-regulation of calmodulins *Calm2* and *Calm3*, but no change in the expression of CaV1.2 (*Cacna1c*), CamkII (*Camk2a/b/d/g*), or NCX (*Slc8a1/2/3*) (Table 1).

We validated the dysregulated genes critical to atrial conduction by reverse transcription PCR (RT-PCR), including the sarcoplasmic reticulum (SR) calcium handling genes *Ryr2*, *Sln*, and *Atp2a2* (SERCA2); connexins *Gja1* and *Gja5*; sodium channels *Scn5a* and *Hcn4*; potassium channel subunits *Kcnj3*, *Kcnd3*, *Kcnn2*, *Kcnj8*, *Kcna5*, *Kcnj2*, *Kcnj5*, and *Abcc9*; and desmoplakin (*Dsp*) (Fig. 3, A to C, and Table 1). Expression of some channels previously linked to AF, including *Kcnq1*, *Kcne1*, *Kcnh2*, and *Scn1b*, were unchanged, indicating specific gene expression changes after *Tbx5* deletion. These data establish a TBX5-directed gene regulatory network for atrial rhythm.

A *PITX2* cis-regulatory element is modulated by TBX5

PITX2 is the most frequently reported human AF GWAS locus and was significantly down-regulated in the left atrium of $Tbx5^{fl/fl};R26^{CreERt2}$ mice (Fig. 3C and Table 1). We hypothesized that the genomic region comprising the AF GWAS signal at *PITX2*, 100 kilo–base pairs (kbp) upstream of the *PITX2* promoter (3, 7, 19, 20), may harbor TBX5-dependent cis-regulatory elements (CREs). To identify candidate regulatory elements, we performed assay for transposase accessible chromatin sequencing (ATAC-seq) (21), which reveals open chromatin, indicative of CRE activity. ATAC-seq was performed on cardiac cells derived from human induced pluripotent stem (iPS) cells. A strong signal indicative of open chromatin was located in a single region upstream of *PITX2*, defining a candidate CRE (hg19 chr4:111,711,915–111,716,751) (Fig. 3D). This region, located 150 to 155 kb 5′ to the *PITX2* transcriptional start site, also harbored marks for DNase I hypersensitivity (22), sequence conservation (22) from ENCODE data, and a canonical TBX5 motif, AGGTG (hg19 chr4: 111,712,182–111,712,186) (Fig. 3D) (23).

We performed high-resolution circular chromosome conformation capture (4C) in murine left atrial tissue to identify genomic regions that interacted with the *Pitx2c* promoter on a genome-wide scale, using the *Pitx2c* promoter as a viewpoint (Fig. 3D). The region syntenic to the candidate CRE made contacts with the *Pitx2c* promoter, indicating a cis-interaction (Fig. 3D). This topology, indicating proximity between the CRE and the *Pitx2c* promoter, supports the region as a candidate *Pitx2* CRE. We then assayed the candidate CRE for TBX5

Author Manuscript Author Manuscript Author Manuscript Author Manuscript

occupancy by ChIP-qPCR in human left atrial tissue. The CRE was significantly enriched 145-fold by TBX5 ChIP compared with a control locus (Fig. 3E), indicating TBX5 occupancy at this CRE in human left atria.

The CRE significantly activated transcription in response to TBX5 expression in HEK293T cells and in the HL-1 atrial cardiomyocyte cell line, which expresses endogenous *Tbx5* (Fig. 3, F and G). A mutant CRE with the T-box binding site ablated (AGGTG to TTTTT) failed to activate expression in response to TBX5 in HEK293T cells ($P = 0.8$ versus blank vector control; *t* test) or in HL-1 cells ($P = 0.53$ versus blank vector control; *t* test) (Fig. 3, F and G). The CRE harbors a common SNP, rs1906595, residing in the T-box binding site. The minor allele (G) (29%) is in perfect linkage disequilibrium with the AF signal tagged by SNP rs2200733 (24). The minor allele (G) completes the canonical T-box binding element (AG**G**TG), whereas the major SNP allele (T) disrupts a central nucleotide of the T-box binding motif (AG**T**GT). We found that the major allele completely abolished CRE activity in response to *TBX5* expression in HEK and HL-1 cells (Fig. 3, F and G). Together, these findings identified a TBX5-dependent CRE at *PITX2* and suggested that TBX5 and PITX2 may co-regulate a common atrial gene regulatory network.

Scn5a, *Gja1*, *Dsp*, *Ryr2*, and *Atp2a2* are co-regulated by TBX5 and PITX2

We hypothesized that TBX5 and PITX2 co-regulate a gene regulatory network essential for atrial rhythm. We compared atrial TBX5-dependent transcripts (Fig. 3, A to C) with PITX2-dependent cardiac transcripts (11). *Scn5a*, *Gja1*, *Dsp*, *Ryr2*, and *Atp2a2* were significantly dysregulated genes in both *Tbx5* and *Pitx2* deletion models. These genes are all critical to atrial conduction, have been previously linked to AF (1, 25, 26), and were shown to be down-regulated in *Tbx5*-mutant adult mouse hearts and up-regulated in *Pitx2*-mutant adult mouse hearts (11).

To test the hypothesis that TBX5 and PITX2 directly co-regulated the expression of these genes, we defined regions with overlapping chromosomal occupancy of both PITX2 and TBX5 from published ChIP data sets (11, 23). Candidate elements were refined by sequence conservation and colocalization of active enhancer marks p300 and H3k27ac (23). The candidate enhancers at all five loci demonstrated significant activation in response to TBX5 expression in HEK293T cells: *Gja1* (mm9 chr10:88816980–88817471), *Ryr2*(mm9chr13:12153077–12153901), *Atp2a2* (mm9 chr5: 122923655–122924226), *Scn5a* (mm9 chr9: 119562160–119563164), and *Dsp* (mm9 chr13: 38244307–38245159) (Fig. 3H). All of the enhancers also showed significant positive responsiveness in HL-1 atrial cardiomyocytes, which was abrogated by mutation of the T-box binding motifs in each regulatory element. PITX2 coexpression blunted TBX5-dependent activation in all cases (Fig. 3H). These findings demonstrate that TBX5 and PITX2 directly and antagonistically co-regulate an atrial rhythm gene regulatory network and describe an incoherent feed-forward loop transcriptional architecture, driven by TBX5 and repressed by PITX2.

Author Manuscript Author Manuscript Author Manuscript Author Manuscript

Reduced *Pitx2* rescued atrial gene expression abnormalities and atrial arrhythmias caused by reduced *Tbx5*

The TBX5/PITX2 incoherent feed-forward loop model predicts that the effects of decreased *Tbx5* dose may be mitigated by decreased *Pitx2* dose. Adult-specific *Tbx5* heterozygous mice ($Tbx5^{fl/+};R26^{CreERt2}$) but not *Pitx2c* heterozygotes ($Pitx2c^{fl/+};R26^{CreERt2}$) showed diminished left atrial expression of *Tbx5* compared with $R26^{CreERt2}$ mice (Fig. 4A and Table 2). $Tbx5^{fl/+};R26^{CreERt2}$ left atria also showed significantly diminished expression of four of the five shared *Tbx5/Pitx2* targets versus control animals: *Scn5a*, *Ryr2*, *Gja1*, and *Atp2a2*. $Pitx2^{fl/+};R26^{CreERt2}$ heterozygotes showed reduced left atrial *Pitx2* and increased *Scn5a*, but no change of *Tbx5*, *Ryr2*, *Gja1*, *Dsp*, or *Atp2a2* expression versus $R26^{CreERt2}$ mice (Fig. 4A and Table 2). *Scn5a*, *Ryr2*, *Gja1*, and *Dsp* expression were all significantly increased in adult-specific compound *Tbx5;Pitx2* heterozygote ($Tbx5^{fl/+};Pitx2^{fl/+};R26^{CreERt2}$) mice compared to *Tbx5* heterozygote mice. Expression of these *Tbx5*/*Pitx2* cotargets was normalized in compound *Tbx5;Pitx2* heterozygotes to their expression in control $R26^{CreERt2}$ mice. Thus, reduced *Tbx5* dose caused decreased expression of *Tbx5/Pitx2* cotargets that was rescued by reduced *Pitx2* dose.

We tested whether atrial rhythm was sensitive to *Tbx5* dosage by examining adult-specific *Tbx5* heterozygotes. $Tbx5^{fl/+};R26^{CreERt2}$ mice demonstrated an irregularly irregular rhythm by surface ECG 2 weeks after TM administration (Fig. 4B and fig. S5A). AF was reproducibly induced in 6 of 7 $Tbx5^{fl/+};R26^{CreERt2}$ mice using catheter-directed intracardiac pacing with either an S1/S2 coupling interval or burst pacing, whereas 0 of 10 $R26^{CreERt2}$ mice experienced AF (Fig. 4E and fig. S5B). Atrial myocytes isolated from $Tbx5^{fl/+};R26^{CreERt2}$ heterozygotes demonstrated inappropriate depolarizations and prolonged atrial APs at both 50% and 90% repolarization (Fig. 4D).

Atrial rhythm was also sensitive to *Pitx2* dosage. Adult-specific *Pitx2* haploinsufficiency ($Pitx2^{fl/+};R26^{CreERt2}$) caused no abnormalities of P-wave duration or PR interval, the time interval between the ECG P wave and QRS, by surface ECG (Fig. 4C). However, $Pitx2^{fl/+};R26^{CreERt2}$ atrial myocytes showed shortened APDs compared to $R26^{CreERt2}$ mice as well as increased APA (Fig. 4D). Furthermore, $Pitx2^{fl/+};R26^{CreERt2}$ mice were susceptible to pacing-induced AF (Fig. 4E and fig. S5B).

Remarkably, the atrial rhythm and cellular electro-physiology abnormalities caused by reduced *Tbx5* dose were all rescued by reduced *Pitx2* dose. Compound adult-specific $Tbx5^{fl/+};Pitx2^{fl/+};R26^{CreERt2}$ mice showed no atrial rhythm instability or other ECG abnormalities, by surface ECG or Poincaré analysis 2 weeks after TM treatment (Fig. 4B and fig. S5A). P-waveduration, prolonged in $Tbx5^{fl/+};R26^{CreERt2}$ mice1 week after TM administration, was rescued in $Tbx5^{fl/+};Pitx2^{fl/+};R26^{CreERt2}$ mice (Fig. 4C and fig. S5A). No discernible PR interval difference was observed between any of these groups (Fig. 4C).

Furthermore, decreased *Pitx2* dose rescued the cellular electrophysiology abnormalities observed in $Tbx5^{fl/+};R26^{CreERt2}$ mice. APD90 prolongation was rescued in $Tbx5^{fl/+};Pitx2^{fl/+};R26^{CreERt2}$ atrial myocytes (Fig. 4D). Additionally, the ectopic depolarizations observed in $Tbx5^{fl/+};R26^{CreERt2}$ were also rescued in $Tbx5^{fl/+};Pitx2^{fl/+};R26^{CreERt2}$ mice (Fig. 4D). Finally, $Tbx5^{fl/+};Pitx2^{fl/+};R26^{CreERt2}$ mice

Author Manuscript Author Manuscript Author Manuscript Author Manuscript

were not susceptible to AF induction by intracardiac pacing (Fig. 4E and fig. S5B). We conclude that the defects in atrial rhythm, AF susceptibility, and cellular electrophysiology caused by reduced *Tbx5* dose were all rescued by reduced *Pitx2* dose.

DISCUSSION

This study links two cardiac transcription factors, TBX5 and PITX2, in a regulatory circuit that controls atrial rhythm. Removal of *Tbx5* profoundly disrupts cardiac channel gene expression and causes primary, spontaneous AF in mice. Despite the high incidence and healthcare burden of AF, there is a limited understanding of the mechanisms underlying its genetic susceptibility. These data provide mechanistic support for a TBX5-driven gene regulatory network in AF risk and link human AF GWAS loci in atrial rhythm control.

We generated a model of primary spontaneous AF in the absence of other cardiac pathology or developmental defects by removing *Tbx5* from the adult mouse. *Tbx5* deletion was sufficient to produce the two components of AF pathophysiology: a “trigger” (ectopic depolarizations) and “substrate” that propagates the trigger (1). Atrial myocytes demonstrated triggered activity, including EADs, DADs, and phase 4 depolarizations. Ex vivo optical mapping revealed slowing of atrial conduction velocity, a substrate allowing arrhythmia propagation through reentry. Trigger and substrate after *Tbx5* removal may explain the resulting primary spontaneous AF, previously elusive in mice.

We then defined a *Tbx5*-dependent network that accounts for both ectopic depolarizations and prolonged APs in adult-specific *Tbx5*-mutant mice. Calcium cycling genes can cause ectopic depolarizations (1), and we observed direct regulation of *Ryr2* and *Atp2a2* by TBX5. We hypothesize that the primary mechanism for the prolonged calcium transient and prolonged AP is the decrement in SERCA2 (*Atp2a2*) expression. Decreased SR Ca^{2+} reuptake resulted in prolongation of cytosolic calcium transient, which in turn may contribute to both prolonged APs and propensity for afterdepolarizations. However, we cannot discount the role of other calcium handling genes, such as *Ryr2* and *Sln*, in the arrhythmogenic cellular electrophysiologic phenotype. The adult-specific *Tbx5*-mutant atrial cardiomyocyte phenotype was rescued by calcium chelation, demonstrating the importance of altered calcium cycling in this setting.

Decreased expression of potassium channel subunits that modulate I_{K1}, I_{Kr}, and I_{to1} currents have been implicated in prolonged APs and abnormal triggering propensity (1). In this vein, expression of *Kcna7*, *Kcnd2*, *Kcnd3*, *Kcng2*, *Kcnj11*, *Kcnj2*, *Kcnj3*, *Kcnj5*, *Kcnj8*, *Kcnk3*, and *Kcnv2* were all significantly decreased after *Tbx5* deletion. Slowed conduction was observed by ex vivo mapping, likely owing to decreased expression of sodium channel gene *Scn5a* and high conductance gap junction connexins *Gja5* and *Gja1*. Consistent with our previous work (27), we did not observe significant expression of *Scn10a* in the adult mouse atria. Thus, *Tbx5* is a driver of rhythm control genes with specific roles, including those that control AP fidelity and myocardial conduction speed. Decreasing the output of this network causes both arrhythmogenic trigger and substrate, providing a mechanism for the observed arrhythmias (Fig. 5).

Author Manuscript Author Manuscript Author Manuscript Author Manuscript

The intersection of *Tbx5*- and *Pitx2*-dependent transcripts identified a subset of essential atrial rhythm genes oppositely regulated by TBX5 and PITX2. We showed here that decreased transcriptional activator *TBX5* or decreased transcriptional repressor *PITX2* causes opposite effects on downstream effector gene regulatory network expression, yet both cause AF susceptibility (11). Thus, AF can occur as a common phenotypic endpoint of opposite perturbations of atrial rhythm gene expression. This observation suggests that substratification of AF patients based on underlying molecular mechanism may afford personalized approaches to this common disorder.

The TBX5-PITX2 loop links critical AF loci and anticipates the identification of genetic variation functionally responsible for AF risk and future genotype-based AF risk stratification. We identified common genetic variation that associates with AF and affects a CRE at *PITX2*. SNP rs1906595 resides within a T-box binding site in the *TBX5*-driven enhancer identified at *PITX2*. AF risk associates with the minor allele and canonical T-box site, and therefore correlates with increased *TBX5*-driven enhancer activity. We speculate that this SNP may increase *PITX2* expression and thereby decrease downstream cardiac channel gene regulatory network expression. This model is consistent with previously published work, in which AF risk SNPs at *PITX2* are associated with increased PITX2 expression (28).

We defined the architecture of an atrial gene regulatory network as an incoherent feed-forward loop, driven by TBX5 and repressed by PITX2 (Fig. 5B). A TBX5-dependent CRE was identified at PITX2, and TBX5- and PITX2-dependent CREs were identified at shared target loci, genes critical to calcium handling (*Ryr2* and *Atp2a2*), rapid depolarization (*Scn5a*), and intracellular communication (*Gja1* and *Dsp*). TBX5 and PITX2 acted directly and antagonistically at the terminal atrial channels of the atrial rhythm gene regulatory network. TBX5/PITX2 antagonism was also observed genetically, in which the physiologic effects of reduced *Tbx5* dose, including decreased expression of critical AF genes, atrial rhythm instability, cellular AP abnormalities, and AF susceptibility, were all rescued by reduced *Pitx2* dose.

The robustness of atrial contraction cycles requires the coordinated expression of genes governing AP fidelity, cell-cell conduction, and free calcium. Variation in these properties is arrhythmogenic (1). Incoherent feed-forward loops impose molecular buffering on terminal regulatory network transcriptional output in response to upstream variance in gene expression (29–31). The *Tbx5/Pitx2* transcriptional architecture is therefore ideal for an atrial gene regulatory network, which must maintain uniform channel gene expression and cellular electrophysiological behavior for normal atrial rhythm for billions of iterations. The *TBX5*-driven *PITX2*-modulated incoherent feed-forward loop provides a molecular logic for atrial rhythm homeostasis.

The transcriptional architecture we describe is based on in vitro studies and in vivo genetic experiments in mice. Although the CREs we tested were human elements or conserved in humans, we have yet to formally observe the incoherent feed-forward loop transcriptional architecture in human atria. Essential future steps include an evaluation of the transcriptional logic of atrial rhythm in humans, the identification of genetic variation in the essential

Author Manuscript Author Manuscript Author Manuscript Author Manuscript

regulatory elements comprising the network, and testing of the functional impact of variants on atrial gene expression and atrial rhythm control. TBX5 and PITX2 do not act in isolation, but are undoubtedly part of a much larger atrial transcriptional complex. How the complete compendium of transcriptional components interact to effect atrial rhythm homeostasis and how genetic variation in the broader atrial gene regulatory network affects atrial rhythm provide opportunities for future studies.

An essential goal of the functional genetics and genomics approaches applied here is to transition from genetic implication of GWAS to molecular mechanism underlying the genetics of AF risk. This work supports a model in which AF is a common endpoint disease process resulting from opposite perturbations of an atrial rhythm control network. This model suggests that a genotype-based personalized approach to the treatment of AF may ultimately be possible. We expect that these and analogous efforts will contribute to improved platforms for disease risk determination and therapeutic stratification.

MATERIALS AND METHODS

Study design

The objective of our study was to investigate the role of TBX5 in atrial rhythm. We used murine models of conditional *Tbx5* deletion, conditional *Pitx2* deletion, and in vitro assays in murine HL-1 cells and human iPS cell–derived cardiomyocytes. Mouse models were chosen for their similarity in cardiac physiology to humans and for the availability of specific genetic tools. Human iPS cell–derived cardiomyocytes were used as an in vitro model of the regulatory loci. Sample sizes were chosen based on power calculations after pilot studies to estimate population mean and SD. All recordings and analyses were conducted in a blinded fashion. Genotype controls were used, and mice randomized into groups when appropriate. Endpoints for studies were selected based on the progression of phenotype. Samples were excluded if replicates were >2 SDs away from the population mean. Replication for specific experiments is in the figure legends.

Generation of conditional Tbx5-deleted mice

Tbx5 was deleted from the adult mouse using the published *Tbx5* floxed allele (*Tbx5*^{fl}) (5), as described in Supplementary Materials and Methods.

ECG recordings

Mice were implanted with subcutaneous telemetry transmitters (ETA-F10; Data Science International) (15). Arrhythmia analysis was carried out using Ponemah Physiology Platform software. Signal average and Poincaré plots were generated with a custom Python script. Catheter-based intracardiac electrophysiology is described in Supplementary Materials and Methods.

Myocyte isolation and AP recordings

To isolate mouse cardiomyocytes, hearts were excised and mounted on a Langendorff apparatus and retrogradely perfused with collagenase type 2 (Worthington Biochemical) in perfusion buffer. Membrane potential was recorded with a ruptured patch current clamp at

Author Manuscript Author Manuscript Author Manuscript Author Manuscript

37°C using an Axon Axopatch 200B amplifier. During recording, cells were perfused in normal Tyrode buffer. APs were triggered using 0.5 nA × 2 ms current clamp pulses. When noted, 5 mM BAPTA-tetrapotassium was included in the pipette solution to abolish cytosolic calcium transients. In all cases, liquid junction potentials were corrected before recording APs. Additional details are in Supplementary Materials and Methods.

RNA-seq and gene expression analysis

Left atrial free wall from $Tbx5^{fl/fl};R26^{CreERt2}$ and $R26^{CreERt2}$ mice was removed, and total RNA was prepared with a TRIzol-based extraction. Sequencing libraries were prepared with Ribo-Zero purification (Illumina) and sequenced on an Illumina HiScanSQ instrument. Samples were sequenced 50 bp single-ended at 10 million to 20 million reads per replicate. Library preparation and sequencing were performed at the University of Chicago Genomics Core Facility. Sequence was aligned to the mouse genome with TopHat2, and differential expression testing was performed with the DESeq2 pipeline. Heatmap and volcano plot were generated in R with the ggplot2 and gplot packages, respectively. Candidate targets were validated with quantitative real-time PCR using exon-spanning primers specific to the gene of interest in a distinct cohort of biological replicates.

ChIP-qPCR of human atrial tissue

Left atrial appendage tissue was collected from three patients undergoing robotic valvular surgery and left atrial appendage plication (Institutional Review Board 12797B). All patients were genotyped as heterozygous at SNP rs1906595. ChIP was performed as previously described using a ChIP-grade TBX5 antibody (sc-17866, Santa Cruz Biotechnology) (32). To determine fold enrichment, we performed qPCR using input controls compared with DNA bound to immunoprecipitated proteins, using primers specific to the site of interest and primers to a site not expected to be enriched. Control primers to the human *GAPDH* locus were as follows: 5′-TACTAGCGGTTTTACGGGCG-3′ and 5′-TCGAACAGGAGGAGCAGAGAGCGA-3′. Primers tiled across the candidate enhancer were 5′-AGTGGCATCAAGACAGCACA-3′ and 5′-CCCCGGATCACCAAATCCAAG-3′, 5′-GTGGGCTGGGTGACTGTATT-3′ and 5′-CCCTGCACTCATGCTGGTTA-3′, and 5′-GCTGCACAACTTAGCTGCAA-3′ and GCCAGAAACAACCTCAAAGCA-3′.

Statistical analysis

For comparison of quantitative metrics of APs, calcium transients, gene expression by quantitative RT-PCR (qRT-PCR), ChIP-qPCR, luciferase response, and ECG parameters, two-tailed *t* tests were used to test significance, with a Bonferroni correction for multiple comparisons when appropriate. For count-based analysis of cellular depolarization events and AF inducibility, two-tailed Fisher's exact tests were used. RNA-seq differential expression was performed with the DE-Seq2 pipeline, with a false discovery rate of <0.05.

Supplementary Material

Refer to Web version on PubMed Central for supplementary material.

Author Manuscript Author Manuscript Author Manuscript Author Manuscript

Acknowledgments

We thank H. Balkhy for assistance in obtaining tissue samples and C.-W. Wu for assistance in cellular electrophysiology studies. This research was supported in part by NIH through resources provided by the Computation Institute and the Biological Sciences Division of the University of Chicago and Argonne National Laboratory, under grant 1S10OD018495-01. We specifically acknowledge the assistance of L. Pesce.

Funding: The study was funded by grants from the NIH (R01 HL114010 to I.P.M; R01HL118761, R01DE023177, and U54 HD083092 to J.F.M.; R01 HL114395 and R01 HL126802 to I.R.E.; and HL128075 to E.M.M.), The Leducq Foundation (FP058566-01-PR, to I.P.M., J.F.M., and V.C.), and the American Heart Association (Established Investigator Award 13EIA14690081 to I.P.M.). This research was supported in part by NIH through resources provided by the Computation Institute and the Biological Sciences Division of the University of Chicago and Argonne National Laboratory, under grant 1S10OD018495-01.

REFERENCES AND NOTES

1. Heijman J, Voigt N, Nattel S, Dobrev D. Cellular and molecular electrophysiology of atrial fibrillation initiation, maintenance, and progression. Circ Res. 2014; 114:1483–1499. [PubMed: 24763466]
2. Nishida K, Nattel S. Atrial fibrillation compendium: Historical context and detailed translational perspective on an important clinical problem. Circ Res. 2014; 114:1447–1452. [PubMed: 24763463]
3. Tucker NR, Ellinor PT. Emerging directions in the genetics of atrial fibrillation. Circ Res. 2014; 114:1469–1482. [PubMed: 24763465]
4. Bruneau BG, Logan M, Davis N, Levi T, Tabin CJ, Seidman JG, Seidman CE. Chamber-specific cardiac expression of *Tbx5* and heart defects in Holt–Oram syndrome. Dev Biol. 1999; 211:100–108. [PubMed: 10373308]
5. Bruneau BG, Nemer G, Schmitt JP, Charron F, Robitaille L, Caron S, Conner DA, Gessler M, Nemer M, Seidman CE, Seidman JG. A murine model of Holt-Oram syndrome defines roles of the T-box transcription factor Tbx5 in cardiogenesis and disease. Cell. 2001; 106:709–721. [PubMed: 11572777]
6. Postma AV, van de Meerakker JBA, Mathijssen IB, Barnett P, Christoffels VM, Ilgun A, Lam J, Wilde AAM, Lekanne Deprez RH, Moorman AFM. A gain-of-function TBX5 mutation is associated with atypical Holt–Oram syndrome and paroxysmal atrial fibrillation. Circ Res. 2008; 102:1433–1442. [PubMed: 18451335]
7. Ellinor PT, Lunetta KL, Albert CM, Glazer NL, Ritchie MD, Smith AV, Arking DE, Müller-Nurasyid M, Krijthe BP, Lubitz SA, Bis JC, Chung MK, Dörr M, Ozaki K, Roberts JD, Smith JG, Pfeufer A, Sinner MF, Lohman K, Ding J, Smith NL, Smith JD, Rienstra M, Rice KM, Van Wagoner DR, Magnani JW, Wakili R, Clauss S, Rotter JI, Steinbeck G, Launer LJ, Davies RW, Borkovich M, Harris TB, Lin H, Völker U, Völzke H, Milan DJ, Hofman A, Boerwinkle E, Chen LY, Soliman EZ, Voight BF, Li G, Chakravarti A, Kubo M, Tedrow UB, Rose LM, Ridker PM, Conen D, Tsunoda T, Furukawa T, Sotoodehnia N, Xu S, Kamatani N, Levy D, Nakamura Y, Parvez B, Mahida S, Furie KL, Rosand J, Muhammad R, Psaty BM, Meitinger T, Perz S, Wichmann H-E, Witteman JCM, Kao WHL, Kathiresan S, Roden DM, Uitterlinden AG, Rivadeneira F, McKnight B, Sjögren M, Newman AB, Liu Y, Gollob MH, Melander O, Tanaka T, Stricker BHC, Felix SB, Alonso A, Darbar D, Barnard J, Chasman DI, Heckbert SR, Benjamin EJ, Gudnason V, Kääb S. Meta-analysis identifies six new susceptibility loci for atrial fibrillation. Nat Genet. 2012; 44:670–675. [PubMed: 22544366]
8. Holm H, Gudbjartsson DF, Arnar DO, Thorleifsson G, Thorgeirsson G, Stefansdottir H, Gudjonsson SA, Jonasdottir A, Mathiesen EB, Njølstad I, Nyrnes A, Wilsgaard T, Hald EM, Hveem K, Stoltenberg C, Løchen ML, Kong A, Thorsteinsdottir U, Stefansson K. Several common variants modulate heart rate, PR interval and QRS duration. Nat Genet. 2010; 42:117–122. [PubMed: 20062063]
9. Tan N, Chung MK, Smith JD, Hsu J, Serre D, Newton DW, Castel L, Soltesz E, Pettersson G, Gillinov AM, Van Wagoner DR, Barnard J. Weighted gene coexpression network analysis of human left atrial tissue identifies gene modules associated with atrial fibrillation. Circ Cardiovasc Genet. 2013; 6:362–371. [PubMed: 23863953]

Author Manuscript Author Manuscript Author Manuscript Author Manuscript

10. Zang X, Zhang S, Xia Y, Li S, Fu F, Li X, Wang F, Zhang R, Tian X, Gao L, Zhang J, Yang Y, Tu X, Wang Q. SNP rs3825214 in *TBX5* is associated with lone atrial fibrillation in Chinese Han population. PLOS One. 2013; 8:e64966. [PubMed: 23717681]
11. Tao Y, Zhang M, Li L, Bai Y, Zhou Y, Moon AM, Kaminski HJ, Martin JF. *Pitx2*, an atrial fibrillation predisposition gene, directly regulates ion transport and intercalated disc genes. Circ Cardiovasc Genet. 2014; 7:23–32. [PubMed: 24395921]
12. Riley G, Syeda F, Kirchhof P, Fabritz L. An introduction to murine models of atrial fibrillation. Front Physiol. 2012; 3:296. [PubMed: 22934047]
13. Alon U. Network motifs: Theory and experimental approaches. Nat Rev Genet. 2007; 8:450–461. [PubMed: 17510665]
14. Ventura A, Kirsch DG, McLaughlin ME, Tuveson DA, Grimm J, Lintault L, Newman J, Reczek EE, Weissleder R, Jacks T. Restoration of p53 function leads to tumour regression in vivo. Nature. 2007; 445:661–665. [PubMed: 17251932]
15. Arnolds DE, Liu F, Fahrenbach JP, Kim GH, Schillinger KJ, Smemo S, McNally EM, Nobrega MA, Patel VV, Moskowitz IP. TBX5 drives *Scn5a* expression to regulate cardiac conduction system function. J Clin Invest. 2012; 122:2509–2518. [PubMed: 22728936]
16. Lang D, Sulkin M, Lou Q, Efimov IR. Optical mapping of action potentials and calcium transients in the mouse heart. J Vis Exp. 2011:e3275.
17. Andrade J, Khairy P, Dobrev D, Nattel S. The clinical profile and pathophysiology of atrial fibrillation: Relationships among clinical features, epidemiology, and mechanisms. Circ Res. 2014; 114:1453–1468. [PubMed: 24763464]
18. Darby AE, Dimarco JP. Management of atrial fibrillation in patients with structural heart disease. Circulation. 2012; 125:945–957. [PubMed: 22354975]
19. Kolek MJ, Parvez B, Muhammad R, Shoemaker MB, Blair MA, Stubblefield T, Kucera GA, Denny JC, Roden DM, Darbar D. A common variant on chromosome 4q25 is associated with prolonged PR interval in subjects with and without atrial fibrillation. Am J Cardiol. 2014; 113:309–313. [PubMed: 24161141]
20. Olesen MS, Holst AG, Jabbari J, Nielsen JB, Christophersen IE, Sajadieh A, Haunsø S, Svendsen JH. Genetic loci on chromosomes 4q25, 7p31, and 12p12 are associated with onset of lone atrial fibrillation before the age of 40 years. Can J Cardiol. 2012; 28:191–195. [PubMed: 22336519]
21. Buenrostro JD, Wu B, Chang HY, Greenleaf WJ. ATAC-seq: A method for assaying vhromatin accessibility genome-wide. Curr Protoc Mol Biol. 2015; 109:21.29.1–21.29.9.
22. ENCODE Project Consortium. An integrated encyclopedia of DNA elements in the human genome. Nature. 2012; 489:57–74. [PubMed: 22955616]
23. He A, Kong SW, Ma Q, Pu WT. Co-occupancy by multiple cardiac transcription factors identifies transcriptional enhancers active in heart. Proc Natl Acad Sci USA. 2011; 108:5632–5637. [PubMed: 21415370]
24. Gudbjartsson DF, Arnar DO, Helgadottir A, Gretarsdottir S, Holm H, Sigurdsson A, Jonasdottir A, Baker A, Thorleifsson G, Kristjansson K, Palsson A, Blondal T, Sulem P, Backman VM, Hardarson GA, Palsdottir E, Helgason A, Sigurjonsdottir R, Sverrisson JT, Kostulas K, Ng MCY, Baum L, So WY, Wong KS, Chan JCN, Furie KL, Greenberg SM, Sale M, Kelly P, MacRae CA, Smith EE, Rosand J, Hillert J, Ma RCW, Ellinor PT, Thorgeirsson G, Gulcher JR, Kong A, Thorsteinsdottir U, Stefansson K. Variants conferring risk of atrial fibrillation on chromosome 4q25. Nature. 2007; 448:353–357. [PubMed: 17603472]
25. Christophersen IE, Ellinor PT. Genetics of atrial fibrillation: From families to genomes. J Hum Genet. 2015; 61:61–70. [PubMed: 25994868]
26. Kostin S, Klein G, Szalay Z, Hein S, Bauer EP, Schaper J. Structural correlate of atrial fibrillation in human patients. Cardiovasc Res. 2002; 54:361–379. [PubMed: 12062341]
27. van den Boogaard M, Smemo S, Burnicka-Turek O, Arnolds DE, van de Werken HJG, Klous P, McKean D, Muehlschlegel JD, Moosmann J, Toka O, Yang XH, Koopmann TT, Adriaens ME, Bezzina CR, de Laat W, Seidman C, Seidman JG, Christoffels VM, Nobrega MA, Barnett P, Moskowitz IP. A common genetic variant within *SCN10A* modulates cardiac *SCN5A* expression. J Clin Invest. 2014; 124:1844–1852. [PubMed: 24642470]

Author Manuscript Author Manuscript Author Manuscript Author Manuscript

28. Martin RI, Babaei MS, Choy MK, Owens WA, Chico TJA, Keenan D, Yonan N, Koref MS, Keavney BD. Genetic variants associated with risk of atrial fibrillation regulate expression of *PITX2*, *CAV1*, *MYOZ1*, *C9orf3* and *FANCC*. J Mol Cell Cardiol. 2015; 85:207–214. [PubMed: 26073630]
29. Goentoro L, Shoval O, Kirschner MW, Alon U. The incoherent feedforward loop can provide fold-change detection in gene regulation. Mol Cell. 2009; 36:894–899. [PubMed: 20005851]
30. Ma W, Trusina A, El-Samad H, Lim WA, Tang C. Defining network topologies that can achieve biochemical adaptation. Cell. 2009; 138:760–773. [PubMed: 19703401]
31. Mangan S, Alon U. Structure and function of the feed-forward loop network motif. Proc Natl Acad Sci USA. 2003; 100:11980–11985. [PubMed: 14530388]
32. Hoffmann AD, Yang XH, Burnicka-Turek O, Bosman JD, Ren X, Steimle JD, Vokes SA, McMahon AP, Kalinichenko VV, Moskowitz IP. *Foxf* genes integrate *Tbx5* and hedgehog pathways in the second heart field for cardiac septation. PLOS Genet. 2014; 10:e1004604. [PubMed: 25356765]
33. Gehrmann J, Berul CI. Cardiac electrophysiology in genetically engineered mice. J Cardiovasc Electr. 2000; 11:354–368.
34. Patel VV, Arad M, Moskowitz IP, Maguire CT, Branco D, Seidman JG, Seidman CE, Berul CI. Electrophysiologic characterization and postnatal development of ventricular pre-excitation in a mouse model of cardiac hypertrophy and Wolff-Parkinson-White syndrome. J Am Coll Cardiol. 2003; 42:942–951. [PubMed: 12957447]
35. Glukhov AV, Flagg TP, Fedorov VV, Efimov IR, Nichols CG. Differential K(ATP) channel pharmacology in intact mouse heart. J Mol Cell Cardiol. 2010; 48:152–160. [PubMed: 19744493]
36. Laughner JI, Ng FS, Sulkin MS, Arthur RM, Efimov IR. Processing and analysis of cardiac optical mapping data obtained with potentiometric dyes. Am J Physiol-Heart C. 2012; 303:H753–765.
37. Simonis M, Kooren J, de Laat W. An evaluation of 3C-based methods to capture DNA interactions. Nat Methods. 2007; 4:895–901. [PubMed: 17971780]
38. van de Werken HJ, Landan G, Holwerda SJ, Hoichman M, Klous P, Chachik R, Splinter E, Valdes-Quezada C, Oz Y, Bouwman BA, Verstegen MJ, de Wit E, Tanay A, de Laat W. Robust 4C-seq data analysis to screen for regulatory DNA interactions. Nat Methods. 2012; 9:969–972. [PubMed: 22961246]
39. Hinson JT, Chopra A, Nafissi N, Polacheck WJ, Benson CC, Swist S, Gorham J, Yang L, Schafer S, Sheng CC, Haghighi A, Homsy J, Hubner N, Church G, Cook SA, Linke WA, Chen CS, Seidman JG, Seidman CE. HEART DISEASE. Titin mutations in iPS cells define sarcomere insufficiency as a cause of dilated cardiomyopathy. Science. 2015; 349:982–986. [PubMed: 26315439]

Author Manuscript
Author Manuscript
Author Manuscript
Author Manuscript

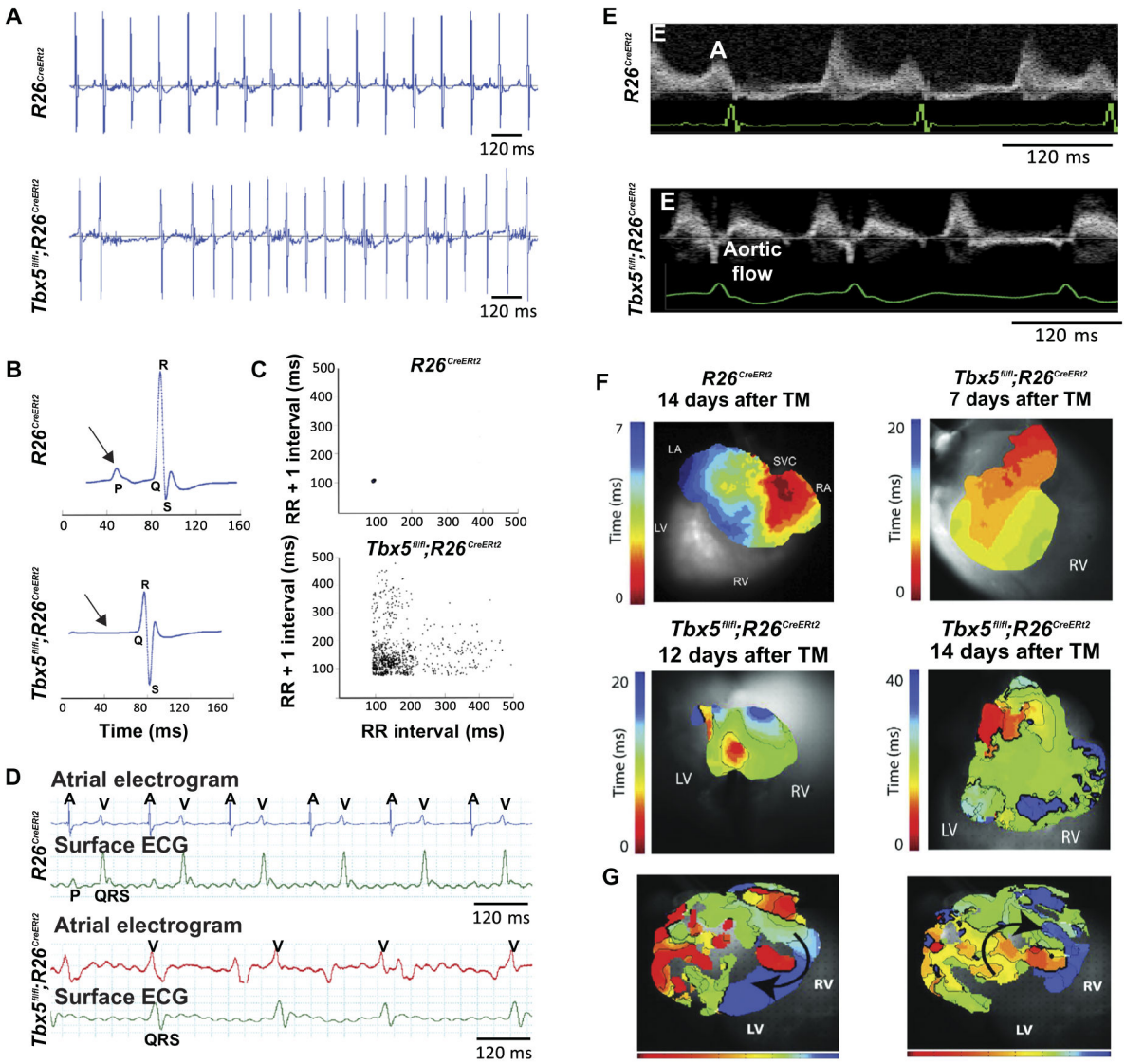

Fig. 1. Removal of Tbx5 from the adult mouse results in spontaneous, sustained AF

(**A**) Representative ambulatory telemetry ECG of $R26^{CreERt2}$ control mice and $Tbx5^{fl/fl};R26^{CreERt2}$ 10 days after receiving TM. ECGs are representative of $n = 24$ $Tbx5^{fl/fl};R26^{CreERt2}$ and $n = 10$ $R26^{CreERt2}$ mice. (**B** and **C**) Signal-averaged ECG waveforms of ~1000 consecutive beats (B) and Poincaré plots of RR interval against the subsequent RR + 1 interval (C) in $R26^{CreERt2}$ ($n = 10$) and $Tbx5^{fl/fl};R26^{CreERt2}$ ($n = 24$) mice. P wave is present in control but absent in $Tbx5^{fl/fl};R26^{CreERt2}$ mice (arrows). Number of mice with absent P wave and irregularly irregular heart rhythm described in A and B, in $Tbx5^{fl/fl};R26^{CreERt2}$ versus $R26^{CreERt2}$. $P = 7.6 \times 10^{-9}$ by two-tailed Fisher's exact test. (**D**) Intracardiac atrial electrogram recordings and surface ECG in $R26^{CreERt2}$ and $Tbx5^{fl/fl};R26^{CreERt2}$ mice. A, atrial electrical signal; V, far field ventricular electrical signal. Data are representative of $n = 6$ $Tbx5^{fl/fl};R26^{CreERt2}$ and $n = 3$ $R26^{CreERt2}$ mice. Number of mice with irregular atrial electrogram in $Tbx5^{fl/fl};R26^{CreERt2}$ versus $R26^{CreERt2}$. $P = 0.012$ by two-tailed Fisher's exact test. (**E**) Pulsed-wave Doppler across mitral valve alongside

Author Manuscript Author Manuscript Author Manuscript Author Manuscript

surface ECG. “A” wave is present in $R26^{CreERt2}$ and absent in $Tbx5^{fl/fl};R26^{CreERt2}$ recordings, indicative of a lack of coordinated atrial contraction. Data are representative of $n = 6$ $Tbx5^{fl/fl};R26^{CreERt2}$ and $n = 3$ $R26^{CreERt2}$ mice. Number of mice with absent “A” wave in $Tbx5^{fl/fl};R26^{CreERt2}$ versus $R26^{CreERt2}$. $P = 0.012$ by two-tailed Fisher’s exact test. (**F**) Representative atrial voltage activation maps from $R26^{CreERt2}$ and $Tbx5^{fl/fl};R26^{CreERt2}$ mice 7, 12, and 14 days after completion of TM treatment. Atrial activation maps demonstrate that conduction waves traverse the atria in ~12 ms at 7 days, ~20 ms at 12 days, and ~40 ms at 14 days after TM treatment. $n = 2$ for each of the three groups. SVC, superior vena cava; RA, right atrium; LA, left atrium; RV, right ventricle; LV, left ventricle. Transatrial conduction speed in $Tbx5^{fl/fl}; R26^{CreERt2}$ versus $R26^{CreERt2}$. $P = 0.02$ by analysis of variance (ANOVA). (**G**) Atrial macro-reentrant pathways observed in $Tbx5^{fl/fl};R26^{CreERt2}$ mice 14 days after TM treatment. Reentrant pathway travels right to left within the posterior atrial wall and left to right through the anterior atrial wall. Images are representative of $n = 2$ mice at 14 days.

Author Manuscript Author Manuscript Author Manuscript Author Manuscript

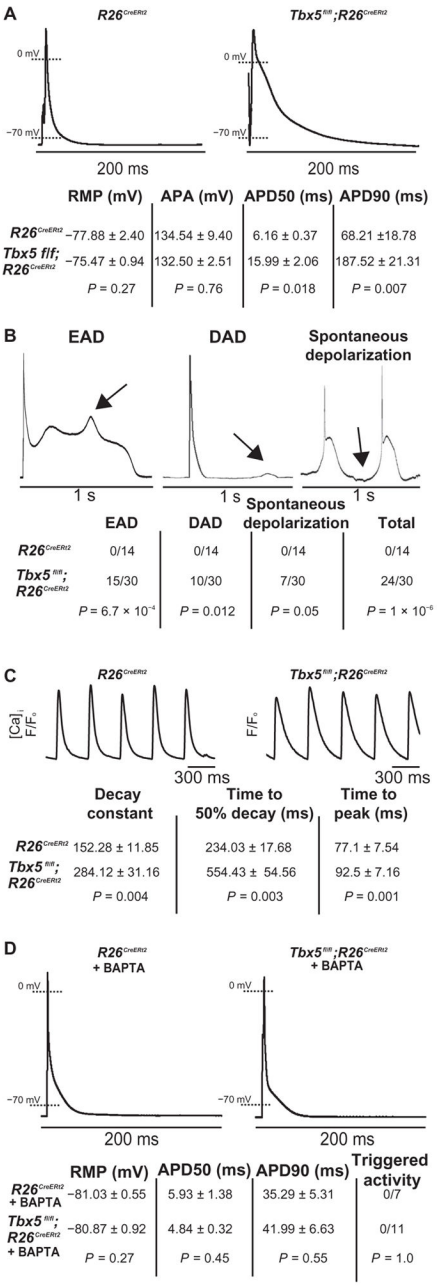

Fig. 2. AP abnormalities in *Tbx5*$^{fl/fl}$;*R26*^{CreERt2} atrial cardiomyocytes are mediated by disrupted calcium handling

(**A**) Representative AP from atrial cardiomyocytes isolated from *R26*^{CreERt2} and *Tbx5*$^{fl/fl}$;*R26*^{CreERt2} mice and the corresponding properties of the APs. Resting membrane potential (RMP), AP amplitude (APA), and APD at 50% (APD50) and at 90% (APD90) repolarization. Data are means ± SEM (*Tbx5*$^{fl/fl}$;*R26*^{CreERt2}, $n = 30$ cardiomyocytes; *R26*^{CreERt2}, $n = 14$ cardiomyocytes; $n > 5$ animals per group). P values were determined by two-tailed t test. (**B**) Representative abnormal depolarization events—EAD, DAD, and spontaneous phase 4 depolarization—observed in atrial cardiomyocytes. Total numbers of abnormal spontaneous events were recorded in *R26*^{CreERt2} ($n = 14$) and *Tbx5*$^{fl/fl}$;*R26*^{CreERt2}

Author Manuscript Author Manuscript Author Manuscript Author Manuscript

($n = 30$) atrial cardiomyocytes from $n > 5$ animals per group. Data are means ± SEM. *P* values were determined by one-tailed Fisher's exact test. (**C**) Representative tracings of calcium release in isolated cardiomyocytes from $R26^{CreERt2}$ and $Tbx5^{fl/fl}; R26^{CreERt2}$ mice. Calcium was imaged with Fluo-4 dye, and myocytes were paced at 1 Hz. Properties of calcium transient spikes, including decay constant (τ), time to 50% decay, and time to peak, were recorded across $R26^{CreERt2}$ ($n = 11$) and $Tbx5^{fl/fl};R26^{CreERt2}$ ($n = 54$) cardiomyocytes from $n > 5$ animals in each group. Data are means ± SEM. *P* values were determined by two-tailed *t* test. (**D**) Representative APs of atrial cardiomyocytes isolated from $R26^{CreERt2}$ and $Tbx5^{fl/fl};R26^{CreERt2}$ adult mutant mice treated with calcium-chelating agent BAP-TA (5 mM). AP properties of these cardiomyocytes were determined, including RMP, APD50, and APD90. Data are means ± SD from $Tbx5^{fl/fl};R26^{CreERt2}$ ($n = 11$) and $R26^{CreERt2}$ ($n = 7$) cardiomyocytes across $n > 3$ animals per group. *P* values were determined by either two-tailed *t* test for continuous measurements or two-tailed Fisher's exact test for count-based measurements (EADs, DADs, spontaneous depolarizations, and total abnormal depolarization events).

Author Manuscript
Author Manuscript
Author Manuscript
Author Manuscript

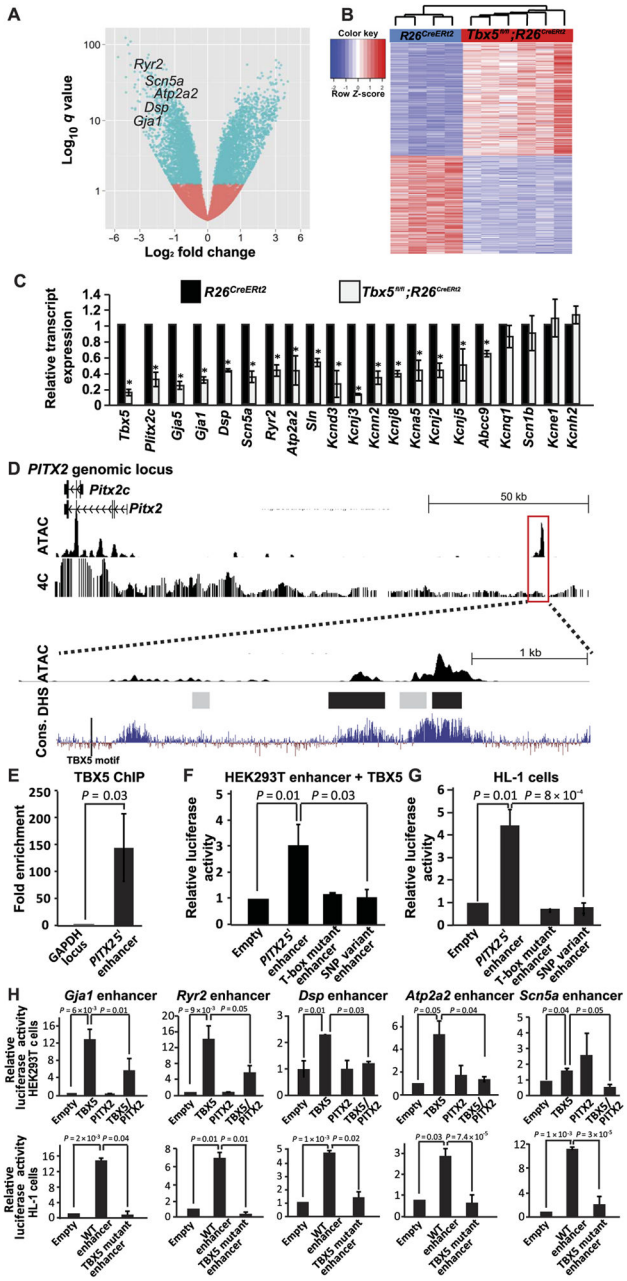

Fig. 3. TBX5-PITX2 gene regulatory network for atrial rhythm control

(**A**) Volcano plot of relative transcript expression from the left atria of *Tbx5*$^{fl/fl}$;*R26*^{CreERt2} versus *R26*^{CreERt2} mice. All significantly misregulated genes ($q < 0.05$) are labeled blue, and all nonsignificant transcripts are in red. TBX5 and PITX2 shared targets labeled. (**B**) Heatmap of all significantly misregulated ($q < 0.05$) transcripts in left atria of *Tbx5*$^{fl/fl}$;*R26*^{CreERt2} ($n = 6$) and *R26*^{CreERt2} ($n = 4$) mice. Cladogram shows clustering of biological replicates. (**C**) Relative gene expression by quantitative polymerase chain reaction (qPCR) of known AF ion channels from left atria. Data are means normalized to *GAPDH* (glyceraldehyde-3-phosphate dehydrogenase) and relative to *R26*^{CreERt2} expression. Data are means ± SEM ($n = 4$ *R26*^{CreERt2} and $n = 7$ *Tbx5*$^{fl/fl}$;*R26*^{CreERt2}). Experiments were

Author Manuscript Author Manuscript Author Manuscript Author Manuscript

performed in technical triplicate. *$P < 0.05$ versus $R26^{CreERt2}$ controls by two-tailed t test. See Table 1 for complete list of genes analyzed. (**D**) *PITX2* genomic locus (hg19) aligned with ATAC-seq of iPS cell–derived cardiomyocytes and 4C with the *PITX2c* promoter as viewpoint. The region cloned for enhancer activity is boxed in red. Below, a smaller scale view of assayed enhancer showing ATAC-seq, Encyclopedia of DNA Elements (ENCODE) deoxyribonuclease (DNase) hypersensitivity (DHS) (darker to lighter gray showing relative strength of DNase signal, darker being stronger signal), and vertebrate conservation (Cons.). The TBX5-binding motif, which should occur by chance every ~1000 nucleotides, is labeled. (**E**) Fold enrichment after TBX5 chromatin immunoprecipitation (ChIP) by qPCR from a control locus and *PITX2* enhancer in the human left atrial appendage. Data are means ± SEM ($n = 3$). (**F** and **G**) In vitro luciferase response assay of the candidate PITX2 regulatory element in human embryonic kidney (HEK) 293T cells cotransfected with TBX5 expression vector or HL-1 atrial cardiomyocytes. Wild-type (WT) enhancer, full mutant variant enhancer lacking the TBX5 binding motif mutant enhancer, and single-nucleotide polymorphism (SNP) rs1906595 variant enhancer are shown. Data are means ± SEM normalized to empty pGl4.23 vector with TBX5 expression ($n = 4$ WT enhancer, $n = 4$ empty, $n = 3$ T-box mutant, $n = 4$ SNP variant). (**H**) In vitro luciferase response assay of candidate TBX5/PITX2 co-regulated elements at *Gja1*, *Ryr2*, *Dsp*, *Atp2a2*, and *Scn5a* in HEK cells cotransfected with TBX5 or TBX5 and PITX2 or HL-1 cardiomyocytes and corresponding T-box mutant enhancers. Data are means ± SEM, normalized to blank vector with corresponding overexpression ($n = 5$ for *Atp2a2* enhancer + TBX5 and *Atp2a2* enhancer + TBX5/PITX2; $n = 3$ for all other groups). Experiments in (E) to (H) were performed in technical triplicate. P values in (E) to (H) were determined by two-tailed t test.

Author Manuscript Author Manuscript Author Manuscript Author Manuscript

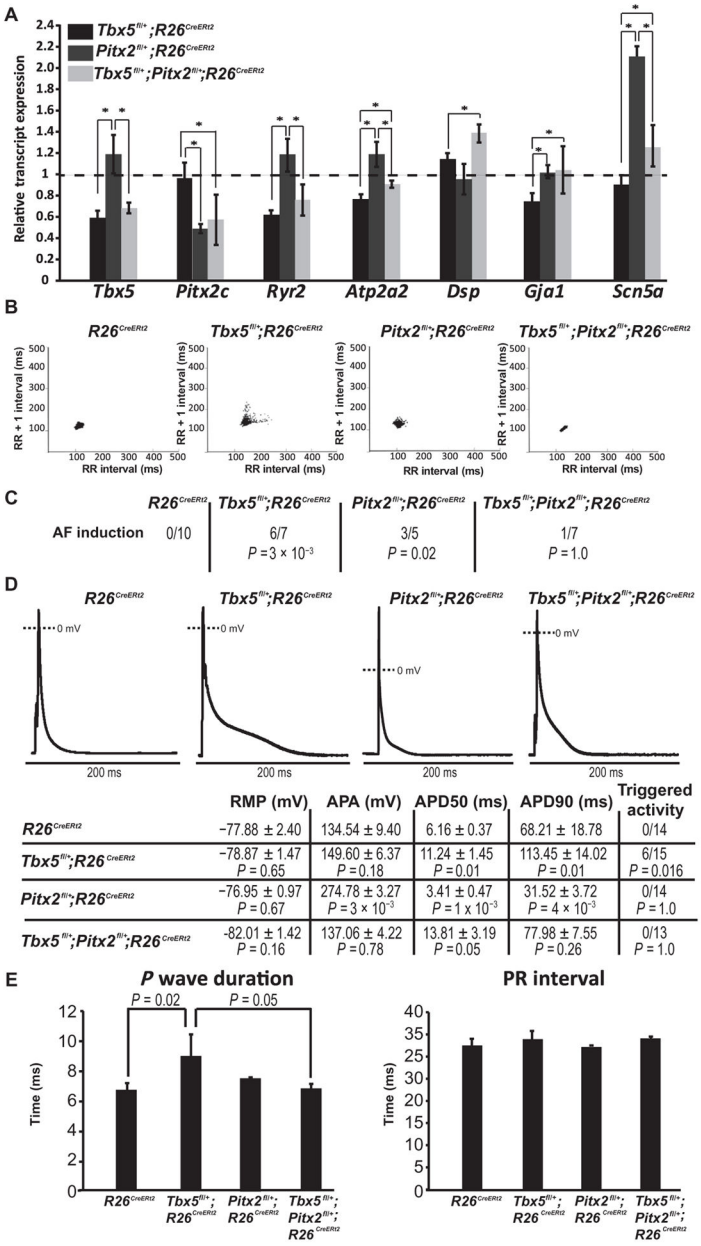

Fig. 4. *Pitx2* haploinsufficiency rescues *Tbx5* haplo-insufficiency in mice

(**A**) Relative transcript expression by qPCR in the left atria from *Pitx2* and *Tbx5* heterozygotes and *Tbx5;Pitx2* compound heterozygotes. Data are means ± SEM normalized to $R26^{CreERt2}$ mice (set as 1) ($n = 11$ $R26^{CreERt2}$; $n = 15$ $Tbx5^{fl/+};R26^{CreERt2}$; $n = 4$ $Pitx2^{fl/+};R26^{CreERt2}$; $n = 8$ $Tbx5^{fl/+};Pitx2^{fl/+};R26^{CreERt2}$). $*P < 0.05$, two-tailed *t* test. Experiments were performed in technical triplicate. (**B**) Representative Poincaré plot of RR interval versus the subsequent RR + 1 interval ($n = 7$ $R26^{CreERt2}$, $n = 6$ $Tbx5^{fl/+};R26^{CreERt2}$, $n = 9$ $Pitx2^{fl/+};R26^{CreERt2}$, and $n = 7$ $Tbx5^{fl/+};Pitx2^{fl/+};R26^{CreERt2}$). (**C**) P-wave duration and PR interval calculated from ambulatory telemetry ECG recordings from mice in (B). *P* values were determined by two-tailed *t* test. Data are means ± SEM. (**D**) Representative AP recordings from atrial myocytes isolated from $R26^{CreERt2}$, $Tbx5^{fl/+};R26^{CreERt2}$,

Author Manuscript Author Manuscript Author Manuscript Author Manuscript

Pitx2$^{fl/+}$;*R26*^{CreERt2}, and *Tbx5*$^{fl/+}$;*Pitx2*$^{fl/+}$;*R26*^{CreERt2} mice. RMP, APA, APD50, and APD90 repolarization were determined from $n > 3$ animals per group ($n = 14$ *R26*^{CreERt2} cells, $n = 15$ *Tbx5*$^{fl/+}$; *R26*^{CreERt2}, $n = 14$ *Pitx2*$^{fl/+}$;*R26*^{CreERt2}, and $n = 13$ *Tbx5*$^{fl/+}$; *Pitx2*$^{fl/+}$;*R26*^{CreERt2}). *P* values were determined versus *R26*^{CreERT2} controls. Inappropriate depolarization *P* values were measured by two-tailed Fisher's exact test; APD90 and APD50 were determined by two-tailed *t* test. (**E**) Pacing induction by intra-atrial pacing of *R26*^{CreERt2} ($n = 10$), *Tbx5*$^{fl/+}$;*R26*^{CreERt2} ($n = 7$), *Pitx2*$^{fl/+}$;*R26*^{CreERt2} ($n = 5$), and *Tbx5*$^{fl/+}$;*Pitx2*$^{fl/+}$;*R26*^{CreERt2} ($n = 7$) mice. *P* values were determined by two-tailed Fisher's exact test.

Author Manuscript Author Manuscript Author Manuscript Author Manuscript

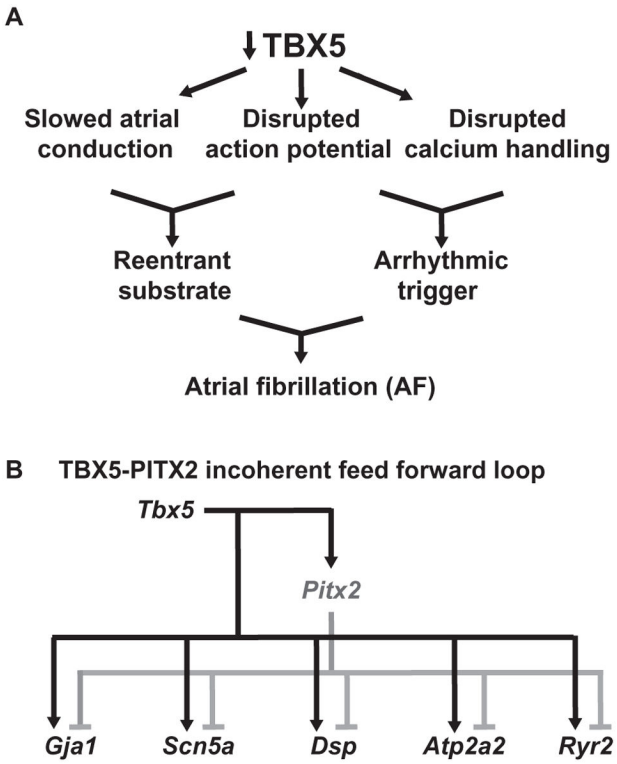

Fig. 5. A TBX5-PITX2 regulatory loop regulates atrial rhythm

(**A**) Loss of TBX5 in the adult atrium leads to slowed atrial conduction, prolonged AP, and disrupted calcium handling, leading to AF trigger and substrate. (**B**) A TBX5-PITX2 incoherent feed-forward loop regulates atrial conduction genes *Scn5a*, *Gja1*, *Ryr2*, *Atp2a2*, and *Dsp*. TBX5 drives PITX2 expression. TBX5 and PITX2 positively and negatively regulate downstream targets. Misregulation of this loop disrupts atrial conduction.

Author Manuscript Author Manuscript Author Manuscript Author Manuscript

Table 1

Gene expression changes in *Tbx5*$^{fl/fl}$;*R26*^{CreERt2} mouse left atria

Gene expression of ion channels implicated in AF and of *Tbx5/Pitx2* cotargets in left atrial tissue from *Tbx5*$^{f/f}$;*R26*^{CreERt2} adult mutant mice normalized to *R26*^{CreERt2} by RNA-seq or qRT-PCR, in independent cohorts. Data are means ± SEM ($n = 4$ *R26*^{CreERt2} and $n = 6$ *Tbx5*$^{f/f}$;*R26*^{CreERt2} for RNA-seq; $n = 4$ *R26*^{CreERt2} and $n = 7$ *Tbx5*$^{fl/fl}$;*R26*^{CreERt2} for qRT-PCR). Nonsignificant changes in the RNA-seq were not validated by real time, with the exception of *Pitx2c*, which was just above significance by RNA-seq.

Gene	*Tbx5*$^{fl/fl}$;*R26*^{CreERt2} versus *R26*^{CreERt2} fold change by RNA-seq	*q* (RNA-seq)	*Tbx5*$^{f/f}$;*R26*^{CreERt2} versus *R26*^{CreERt2} fold change by qRT-PCR	*P* (qRT-PCR)
Pitx2c	0.53	0.07	0.22 ± 0.09	0.03
Gja5	0.05	3×10^{-4}	0.23 ± 0.05	2.49×10^{-6}
Gja1	0.24	3×10^{-4}	0.30 ± 0.04	1.06×10^{-5}
Dsp	0.36	3×10^{-4}	0.44 ± 0.05	1.99×10^{-8}
Scn5a	0.30	3×10^{-4}	0.34 ± 0.07	1.06×10^{-5}
Ryr2	0.22	3×10^{-4}	0.42 ± 0.07	2.14×10^{-6}
Atp2a2	0.42	3×10^{-4}	0.42 ± 0.17	0.002
Sln	0.41	3×10^{-4}	0.52 ± 0.05	1.2×10^{-4}
Kcnd3	0.67	7×10^{-3}	0.25 ± 0.17	0.002
Kcnj3	0.14	3×10^{-4}	0.12 ± 0.01	9.56×10^{-12}
Kcnn2	0.77	0.10	0.33 ± 0.08	4.83×10^{-5}
Kcnj8	0.67	7×10^{-3}	0.38 ± 0.04	3×10^{-6}
Kcna5	0.78	0.04	0.42 ± 0.13	4×10^{-4}
Kcnj2	0.60	3×10^{-4}	0.42 ± 0.09	1.4×10^{-4}
Kcnj5	0.21	3×10^{-4}	0.49 ± 0.2	4.7×10^{-5}
Abcc9	0.58	3×10^{-4}	0.63 ± 0.04	1.7×10^{-5}
Cacna1c	0.95	0.88		
Camk2a/b/d/g	0.24/0.83/0.59/1.25	0.11/1/0.2/1		
Slc8a1/2/3	0.81/3.08/0.61	0.18/1/1		
Calm2/3	1.27/1.44	$0.03/4 \times 10^{-4}$		

Author Manuscript Author Manuscript Author Manuscript Author Manuscript

Table 2

Gene expression changes in *Tbx5$^{fl/+}$;R26^{CreERt2}*, *Pitx2$^{fl/+}$;R26^{CreERt2}*, and *Tbx5$^{fl/+}$;Pitx2$^{fl/+}$; R26^{CreERt2}* mouse left atria

Gene expression TBX5/PITX2 shared targets in left atrial tissue normalized to *R26^{CreERt2}* by qRT-PCR, in independent cohorts. Data are means ± SEM (n = 4 *R26^{CreERt2}* and n = 6 *Tbx5$^{f/f}$;R26^{CreERt2}* for RNA-seq; n = 4 *R26^{CreERt2}* and n = 7 *Tbx5$^{fl/fl}$; R26^{CreERt2}* for qRT-PCR).

	***Tbx5$^{f/+}$;R26^{CreERt2}* fold change**	***Pitx2$^{f/+}$;R26^{CreERt2}* fold change**	***Tbx5$^{f/+}$;Pitx2$^{fl/+}$;R26^{CreERt2}* fold change**
Tbx5	0.55 ± 0.06 *	1.11 ± 0.17 †	0.64 ± 0.05 *
Pitx2c	0.91 ± 0.13	0.45 ± 0.10 *†	0.54 ± 0.22 *
Ryr2	0.59 ± 0.04 *	1.12 ± 0.15 †	0.72 ± 0.14 *
Atp2a2	0.73 ± 0.05 *	1.10 ± 0.11 †	0.86 ± 0.08 †
Dsp	1.07 ± 0.07	0.88 ± 0.14	1.31 ± 0.21
Gja1	0.70 ± 0.04 *	0.95 ± 0.06 †	0.98 ± 0.03 †
Scn5a	0.85 ± 0.08 *	1.95 ± 0.10 *†	1.18 ± 0.23 †

* $P < 0.05$ versus *R26^{CreERt2}*

† $P < 0.05$ versus *Tbx5$^{fl/+}$*;

R26^{CreERt2}. n = 11 *R26^{CreERt2}*; n = 15 *Tbx5$^{fl/+}$;R26^{CreERt2}*; n = 4 *Pitx2$^{fl/+}$;R26^{CreERt2}*; n = 8 *Tbx5$^{fl/+}$;Pitx2$^{fl/+}$;R26^{CreERt2}*. For *Tbx5$^{fl/+}$;R26^{CreERt2}* versus *R26^{CreERt2}* *Tbx5:* $P = 1.5 \times 10^{-5}$; *Pitx2c:* $P = 0.86$; *Scn5a:* $P = 0.028$; *Ryr2:* $P = 3.98 \times 10^{-5}$; *Gja1:* $P = 6.98 \times 10^{-3}$ and *Atp2a2:* $P = 5.5 \times 10^{-3}$. For *Pitx2$^{fl/+}$;R26^{CreERt2}* versus *R26^{CreERt2}* *Pitx2c:* $P = 0.05$; *Scn5a:* $P = 0.03$; *Tbx5:* $P = 0.47$; *Ryr2:* $P = 0.44$; *Gja1:* $P = 0.52$; *Atp2a2:* $P = 0.60$. For *Tbx5$^{fl/+}$;Pitx2$^{fl/+}$;R26^{CreERt2}* versus *Tbx5$^{fl/+}$;R26^{CreERt2}* *Tbx5:* $P = 0.56$; *Scn5a:* $P = 7.5 \times 10^{-3}$; *Ryr2:* $P = 0.01$; *Gja1:* $P = 0.02$; *Atp2a2:* $P = 0.19$; *Dsp:* $P = 0.05$. *Tbx5$^{fl/+}$;Pitx2$^{fl/+}$;R26^{CreERt2}* versus *R26^{CreERt2}* *Scn5a:* $P = 0.58$; *Ryr2:* $P = 0.07$; *Gja1:* $P = 0.99$; *Atp2a2:* $P = 0.19$; *Dsp:* $P = 0.31$. By two-tailed t test. Experiments performed in technical triplicate.